Kenneth A. Miles, MBBS, FRCR, MSc • Michael P. Hayball, MA, MSc
Adrian K. Dixon, MD, FRCP, FRCR

Functional Images of Hepatic Perfusion Obtained with Dynamic CT[1]

A dynamic computed tomographic (CT) technique for separate quantification of arterial and portal components of liver perfusion with functional imaging was developed and used to study 24 livers. A single-location dynamic sequence was performed after intravenous administration of a 50-mL bolus of contrast medium. The time to maximum splenic enhancement was used to differentiate arterial and portal phases, and the maximal slopes of the liver time-density curve in each phase were used to calculate both arterial and portal perfusion. The arterial/total perfusion ratio was also calculated. The values of these parameters for individual pixels were used to create functional images. Arterial perfusion was increased in patients with metastases and cirrhosis. Portal perfusion was reduced in patients with cirrhosis. Functional images were successfully created in all but one case. The technique enables quantification and functional mapping of several perfusion parameters with a spatial resolution greater than that achieved with other imaging techniques.

Index terms: Computed tomography (CT), image processing, 761.12113 • Liver, blood supply • Liver, cirrhosis, 761.794 • Liver neoplasms, 761.33

Radiology 1993; 188:405–411

DETERMINATION of organ blood flow during the first pass of incompletely extracted radiotracers has been described and validated by Peters et al (1,2). The technique can be successfully applied to dynamic computed tomography (CT) after injection of a bolus of contrast media, with derivation of an equation for perfusion (in milliliters of blood flow per minute per milliliter of tissue), as follows (3) (see Appendix):

$$\frac{\text{maximum rate of tissue enhancement (Hounsfield units per minute)}}{\text{peak arterial enhancement (Hounsfield units)}}. \quad (1)$$

If this equation is used to calculate perfusion pixel by pixel, it is possible to generate a perfusion map with a spatial resolution higher than that achievable with radionuclide techniques (4).

Application of this technique to the liver is complicated by the biphasic pattern of enhancement resulting from contrast medium arriving first with the hepatic arterial blood and then slightly later via the hepatic portal system.

Various radionuclide techniques have been used in an attempt to evaluate these two components separately, with the time of peak splenic activity used to differentiate arterial from portal phases (5–7). The techniques have been of value for studying patients with liver metastases and hepatic cirrhosis and for patients who have undergone liver transplantation. However, because of the limited resolution of the gamma camera, such techniques have enabled the study of data from only large regions of interest (ROIs) over the right lobe of the liver, and, although functional images of hepatic blood flow parameters have been produced (8), they have had poor spatial resolution. It also has not been possible to study the left lobe of the liver because of overlap of the aorta and inferior vena cava, thereby including substantial amounts of vascular activity within the left lobe ROI.

The aim of this study was to develop a dynamic CT technique that can enable determination of hepatic arterial and portal perfusion and the arterial/total perfusion ratio (hepatic perfusion index [HPI]). The technique would be applicable to the left lobe of liver, as the transaxial format of the images allows differentiation from the large vessels. These values could then be measured for individual pixels and displayed as functional images with high spatial resolution.

MATERIALS AND METHODS

Subjects

Twenty-four patients underwent dynamic CT of the liver as part of the CT assessment of known or suspected liver disease. One patient was excluded from analysis because of excessive respiratory movement. Of the remaining 23 patients, five had normal livers, 10 had cirrhosis, and four had hepatic metastases; four patients had miscellaneous diseases. The five patients with normal livers served as control subjects. The control subjects included three patients who were suspected of having hepatic metastases; results of CT and ultrasound (US) were normal in these patients, and findings at liver function tests and follow-up CT examinations performed 6 months later were normal. Hepatic cirrhosis had been suspected in one control subject but was not confirmed at subsequent liver biopsy. The last control subject had a benign islet cell tumor of the pancreas, normal results at liver function tests, and a morphologically normal liver.

In the 10 patients with cirrhosis, the diagnosis was confirmed at histologic examination after liver biopsy. Three patients

[1] From the Departments of Nuclear Medicine (K.A.M.), Radiology (K.A.M.), and Medical Physics (M.P.H.) and the University Department of Radiology (A.K.D.), Addenbrooke's Hospital, Hills Rd, CB2 2QQ Cambridge, England. From the 1992 RSNA scientific assembly. Received December 4, 1992; revision requested January 15, 1993; revision received March 4; accepted March 18. **Address reprint requests to** K.A.M.
© RSNA, 1993

Abbreviations: HAR = hepatic arterial ratio, HPI = hepatic perfusion index, ROI = region of interest, TDC = time-density curve.

had alcoholic cirrhosis, four had biliary cirrhosis, and one each had idiopathic cirrhosis, Wilson disease, and Gaucher disease. Two cirrhotic livers also contained a hepatocellular carcinoma; one was confirmed after biopsy and one was discovered because of an increase in α-fetoprotein level. In the four patients with metastases, the diagnosis was confirmed at laparotomy in three. The fourth patient had a progressive focal liver lesion after surgical excision of a colonic carcinoma. The patients with miscellaneous diseases included two liver transplant recipients, one patient with postanesthetic hepatitis (diagnosed at histologic examination), and one patient with a focal area of fat infiltration in the liver that had remained unchanged at serial examinations performed during an 18-month period.

Eight subjects (two control subjects, six patients with cirrhosis) also underwent dynamic colloid scintigraphy with measurement of the ratio of arterial to total liver blood flow (hepatic arterial ratio [HAR]) within 1 week of the dynamic CT examination, enabling validation of the CT method of determining the HPI.

Data Acquisition

Single-location dynamic sequences were performed with a Somatom Plus CT system (Siemens, Erlangen, Germany) at the level of the liver after injection of a 50-mL bolus of iopamidol (300 mg/mL) (Niopam; Merck, Hampshire, England). Iopamidol was injected as rapidly as possible by hand (8–10 seconds) into an antecubital vein. A 10-mm section thickness was used. Data acquisitions of 1-second duration were performed at 0 second and 7, 10, 13, 16, 21, 26, 31, 37.5, and 44 seconds after the injection of contrast medium. The patient was instructed to breathe as quietly as possible during the examination. The level for the sequence was chosen either to include a focal abnormality identified on unenhanced images or to include left and right lobes of the liver and the spleen in patients with diffuse liver disease. Some images were from examinations performed to evaluate another organ (eg, the pancreas), and the liver happened to be included in the section. The images were subsequently compressed into a 256 × 256 matrix and transferred to a computer workstation (Archimedes; Acorn, Cambridge, England).

ROI Analysis

Time-density curves (TDCs) were created from circular ROIs with a minimum size of 50 pixels (256 × 256 matrix) drawn over the aorta, right lobe of liver, left lobe of liver, and spleen. The ROIs were as large as possible to minimize noise but with a sufficient margin from the edge of the structure to avoid partial-volume effects. The time to peak splenic enhancement was used to differentiate the arterial and portal phases on the TDCs from the liver. When the spleen was not included in the section, the time to peak pancreatic or renal cortical enhancement was used. On the basis of the general equation for measurement of tissue perfusion from dynamic CT data as described by Miles (3) (Eq [1]), hepatic arterial perfusion (in milliliters per minute per milliliter of tissue) was determined by dividing the maximum rate of enhancement of the liver *before* the splenic peak by the peak aortic enhancement. Similarly, portal perfusion (in milliliters per minute per milliliter of tissue) was calculated by dividing the maximum slope *after* the time of peak splenic enhancement by the peak aortic enhancement (Fig 1). The HPI, which expresses the proportion of hepatic perfusion that is arterial, is analogous to the same parameter used in dynamic colloid scintigraphy (5,7), and is given by the equation

$$\text{HPI} = \frac{\text{arterial perfusion}}{(\text{arterial perfusion} + \text{portal perfusion})} \times 100\% \quad (2)$$

These values were compared for control subjects and patients with cirrhosis, metastasis, and miscellaneous disease by using the Wilcoxon rank sum test. The times to peak splenic enhancement and to the maximal increases in arterial and portal enhancement were also noted. ROIs were also created over focal liver lesions and the arterial perfusion calculated by using Equation (1).

Functional Images

Software was developed to create a TDC for each pixel of the 256 × 256 matrix with use of the attenuation values from corresponding pixels in each image of the dynamic sequence. Any pixels containing fat or bone were eliminated by excluding pixels with attenuation values of less than 0 HU or greater than 400 HU. These pixels were assigned zero perfusion. (If peak arterial enhancement were greater than 400 HU, these pixels would also be eliminated but the true value of peak aortic enhancement would be used for the perfusion calculations.) With use of the peak aortic enhancement and the time of peak splenic enhancement derived from the ROI analysis, values for hepatic arterial perfusion, portal perfusion, and HPI were determined for each liver pixel from their individual TDCs. These values were then used to create functional images of each parameter displayed by means of a 256-element color scale. Instead of scaling the images to the maximum value, all functional images were displayed with the following color scales to enable direct comparisons: For HPI images, black represented 0% arterial flow and red represented 100% arterial flow. For arterial and portal perfusion images, black indicated perfusion of 0 mL/min/mL and red indicated perfusion of 2.5 mL/min/mL. Any tissues with perfusion values greater than 2.5 mL/min/mL would therefore appear white.

The images were evaluated visually to detect regional variations in hepatic perfusion parameters and to characterize focal abnormalities.

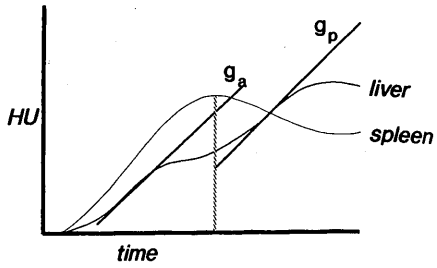

Figure 1. Hepatic and splenic TDCs show biphasic enhancement of the liver resulting from the contrast medium arriving in arterial and portal phases. g_a = maximum slope of liver TDC before peak splenic enhancement, g_p = maximum slope after peak splenic enhancement.

Table 1
Time to Maximal Arterial and Portal Slopes of Liver TDCs and Their Relationship to the Time of Peak Splenic Enhancement

Parameter	Mean (sec)	Range (sec)
Time to maximal slope during arterial phase	15.3	10.5–25.9
Time to maximal slope during portal phase	30.6	20.7–36.8
Time to peak splenic enhancement	24.4	15.4–33.4
Time from maximal arterial slope to splenic peak	9.1	1.8–22.9
Time from splenic peak to maximal portal slope	6.2	1.0–21.3
Time between maximal arterial and portal slopes	15.3	4.0–26.2

Table 2
Perfusion Measurements from Seven Focal Liver Lesions

Lesion Type	Perfusion (mL/min/mL)
Hepatocellular carcinoma	0.70
Hepatocellular carcinoma	0.59
Metastasis	0.63
Metastasis	0.56
Metastasis	0.38
Metastasis	0.19
Focal fat	0.10

Dynamic Colloid Scintigraphy

A large-field-of-view gamma camera was positioned posteriorly over the liver and spleen and, after injection of a bolus of 150–350 MBq of technetium-99m–labelled colloid, a series of 2-second frames were acquired over 5 minutes with a 64 × 64 matrix. The splenic uptake method of analysis, as described by Wraight et al (9),

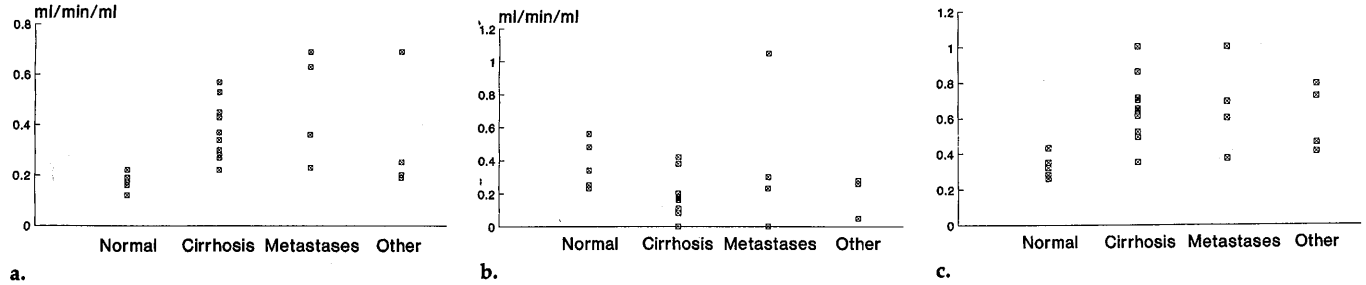

Figure 2. (a) Hepatic arterial perfusion indexes, (b) portal perfusion indexes, and (c) HPIs from the right lobe for various liver conditions.

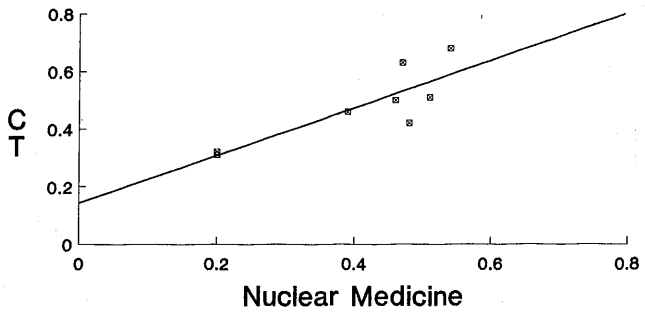

Figure 3. Correlation between dynamic colloid scintigraphy–determined HAR and CT-determined HPI.

was used to determine the HAR from an ROI over the right lobe of the liver. The HPI as derived from the CT method was compared with the scintigraphic value of HAR for each of the eight patients.

RESULTS

ROI Analysis

Figure 2 demonstrates the differences in right lobe arterial and portal perfusion and HPI derived from ROI analysis for the control subjects and the patients with cirrhosis, metastases, and miscellaneous disease. The median HPI was significantly higher in patients with cirrhosis (0.65), metastases (0.65), and miscellaneous disease (0.59) than in the control subjects (0.32; $P < .005$, .05, and .05, respectively). The portal perfusion index was significantly lower in patients with cirrhosis (0.17 mL/min/mL) than in control subjects (0.34 mL/min/mL; $P < .02$), but this was not so for the other groups. Arterial perfusion was significantly higher in patients with cirrhosis (0.36 mL/min/mL; $P < .002$) and metastases (0.50 mL/min/mL; $P < .02$) when compared with that in control subjects (0.17 mL/min/mL). The difference between the groups was clearest for arterial perfusion, with portal perfusion demonstrating greater variability. The mean values and ranges of the times to peak splenic enhancement and the times to maximal rates of arterial and portal enhancement (and the intervals between these times) are given in Table 1.

Table 2 lists the arterial perfusion values observed in the seven focal liver lesions studied. Hepatocellular carcinomas had the highest perfusion values. Patients with metastases demonstrated a wide range of perfusion values; the patient with a focal area of fat infiltration had low perfusion. Patients with hepatocellular carcinoma and all but one of the patients with metastases had arterial perfusion values greater than those in the control subjects.

Comparison of CT and Dynamic Colloid Scintigraphy

Figure 3 compares the results of dynamic colloid scintigraphy and dynamic CT. There was a significant correlation ($P < .001$, $r = .94$) between the HAR and the CT measurement of HPI from the right lobe of liver.

Functional Images

Functional images of arterial and portal perfusion and HPI were successfully obtained in all 23 subjects. Perfusion parameters were calculated for all voxels in the image except air, fat, and bone, which were eliminated by excluding pixels with initial attenuation values less than 0 HU or greater than 400 HU. Thus, perfusion values for voxels containing nonhepatic structures are also displayed. Although the portal perfusion index and HPI for such pixels have little physiologic importance, they were included to maintain spatial orientation. Three representative cases are described below.

Case 1: normal liver.—A 60-year-old man presented with epigastric pain, diarrhea, and weight loss. He was found to have a carcinoma of the sigmoid colon at barium enema examination. Results of CT, performed to exclude metastases, were normal. Subsequent laparotomy confirmed a colonic carcinoma, which was resected, and a normal liver. The patient was well, and results of a liver function test performed 6 months later were normal.

Figure 4 demonstrates the normal arterial perfusion, portal perfusion, and HPI images. Mean values in the right lobe for these parameters are 0.17 mL/min/mL, 0.48 mL/min/mL, and 0.26, respectively.

Case 2: idiopathic cirrhosis and hepatocellular carcinoma.—A 68-year-old woman with histologically proved idiopathic cirrhosis was determined to have bleeding esophageal varices. The hemorrhage settled with conservative management, but tests revealed an elevated serum α-fetoprotein level at 41 μg/L (normal, <12 μg/L). Conventional CT scans demonstrated typical features of cirrhosis, with a hepatocellular carcinoma in the right lobe (Fig 5a).

Figure 5b–5d demonstrates the perfusion images. The HPI is increased throughout the liver (it is typically 0.67), including the hepatocellular carcinoma, with increased arterial (0.4 mL/min/mL) and decreased portal (0.2 mL/min/mL) perfusion. The hepatocellular carcinoma showed greatest perfusion peripherally, with low values in the presumed necrotic center (mean perfusion, 0.65 mL/min/mL).

Case 3: hepatic metastases.—A 47-year-old man presented with upper abdominal pain and was found to have a gastric ulcer. Endoscopic biopsy revealed adenocarcinoma. At laparotomy, an antral carcinoma was confirmed and a liver metastasis was seen. Partial gastrectomy was performed. CT was performed to docu-

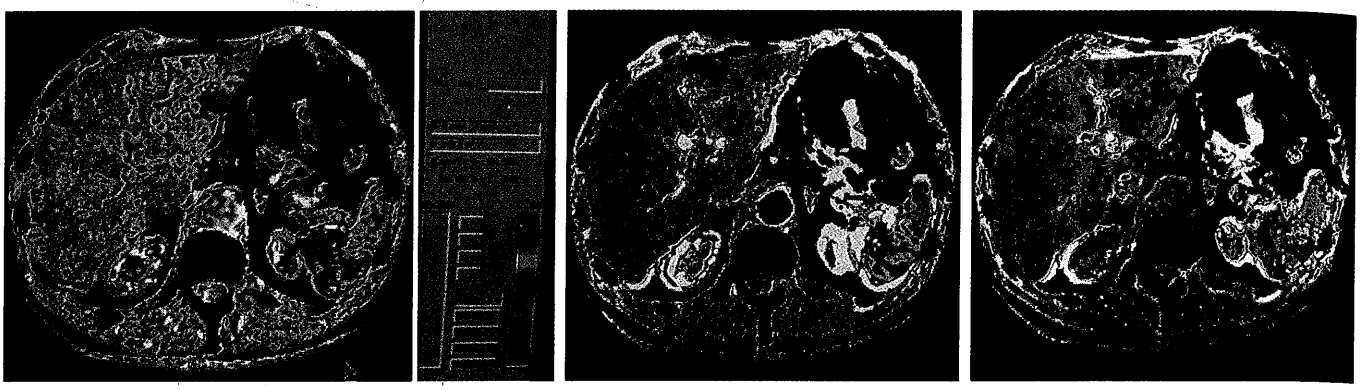

b. c. d.

Figure 4. Images of normal liver. **(a)** Unenhanced CT scan, **(b)** HPI image, **(c)** arterial perfusion image, and **(d)** portal perfusion image.

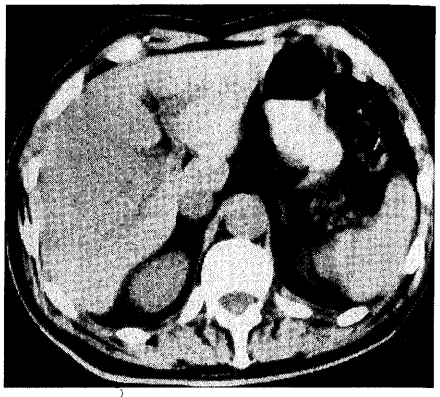

a.

ment disease extent before chemotherapy.

Figure 6 demonstrates an unenhanced CT scan and the corresponding perfusion images. The metastasis has high values on the HPI image but low values on the portal perfusion image. The perfusion is also abnormal in the areas that do not appear to contain metastases on the conventional CT image, with an increase in HPI (0.4–0.55) and arterial perfusion (0.6–0.85 mL/min/mL).

DISCUSSION

To our knowledge, the quantification of hepatic arterial and portal perfusion with dynamic CT with creation of functional images has not been previously described. Although dynamic CT has been used for evaluation of tissue perfusion (3,10–14), including functional imaging (4,15,16), these techniques have not been systematically applied to the liver and would not allow differentiation of arterial and portal phases. Partanen (17) has described differences in TDCs between normal and cirrhotic livers, but again the frequency of data acquisition was too low for differentiation of arterial and portal phases.

The statistically significant correlation between dynamic colloid scintigraphy and dynamic CT has provided reasonable direct validation of the CT technique for determining the HPI. Portal perfusion is underestimated with the CT method because there is some loss of contrast medium into the extracellular space of the spleen and gut during its first pass through these organs before passage to the liver in the portal blood. Thus, CT values for HPI are generally higher than the corresponding HAR values from scintigraphy.

The fact that the CT technique has demonstrated changes in liver perfusion parameters in disease states provides further clinical validation and indicates potential clinical uses of the technique. The increase in HPI that occurs in cirrhosis is due to not only a decrease in portal perfusion as a result of portal hypertension but also to a rise in arterial perfusion (Fig 1). This reciprocal relationship has been previously demonstrated with use of flow meters in an experimental dog model (18) and in a human at surgery (19) and has been suggested as the mechanism for transient regional variations in liver attenuation after intravascular administration of contrast medium in portal vein branch thrombosis and focal liver lesions (20–23).

Liver tumors, whether primary hepatocellular carcinoma or metastatic deposits, have a blood supply derived almost exclusively from the arterial rather than portal circulation and, hence, appear as areas of increased HPI on the functional images. As would be expected, measured perfusion was higher in the hepatocellular carcinomas than in the metastases with this CT technique. In livers that contain metastases, the areas that appear morphologically unaffected display abnormal hemodynamics, with an increase in arterial perfusion and HPI. There are many possible explanations for this. Radionuclide studies of liver blood flow in patients with colonic cancer have demonstrated a group of patients with an increased HPI in whom metastases were not visible on images or at surgery (24). Such patients have a greater probability of subsequently developing hepatic metastases than do those with normal flow characteristics, and it is proposed that the presence of "micrometastases" (eg, metastases too small to visualize) causes alterations in liver hemodynamics. Thus, in patients with visible metastases, the apparently unaffected portions of liver could contain micrometastases. A further explanation would be, as postulated by Itai et al (20) for transient lobar attenuation differences in patients with focal liver lesions, that the presence of a hypervascular lesion within a region of the liver increases the arterial flow not just to the lesion itself but to the whole of that liver region as a result of a steal phenomenon. Alternatively, increasing pressure within a liver segment or lobe containing metastases may reduce portal flow to that portion of liver with a reciprocal rise in arterial perfusion.

Other methods that allow separate evaluation of arterial and portal flow within the liver include dynamic colloid scintigraphy, Doppler US, and magnetic resonance (MR) imaging. As discussed earlier, scintigraphy cannot accurately demonstrate regional variations in flow parameters or depict the left lobe. Furthermore, although the arterial/total flow ratio can be obtained, arterial and portal components cannot be quantified separately. Doppler US is largely limited to evaluating large and medium-size vessels and, thus, the ability to demonstrate regional variations is limited to perhaps left and right hepatic arteries

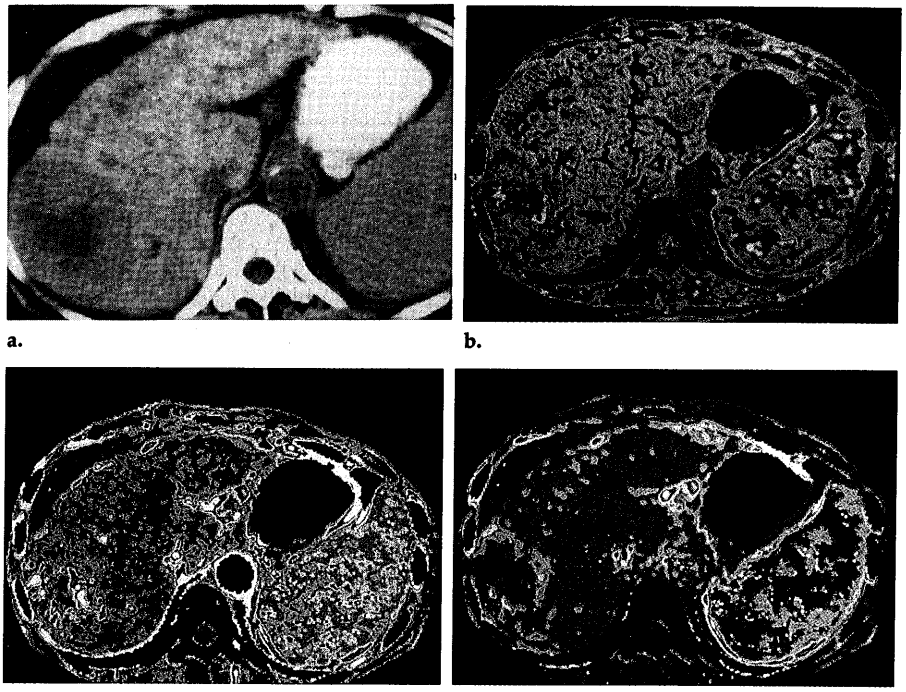

Figure 5. Idiopathic cirrhosis with hepatocellular carcinoma. **(a)** Unenhanced CT scan, **(b)** HPI image, **(c)** arterial perfusion image, and **(d)** portal perfusion image. The HPI is elevated throughout the liver. Note the high arterial perfusion in the periphery of the tumor, with lower values in the necrotic center.

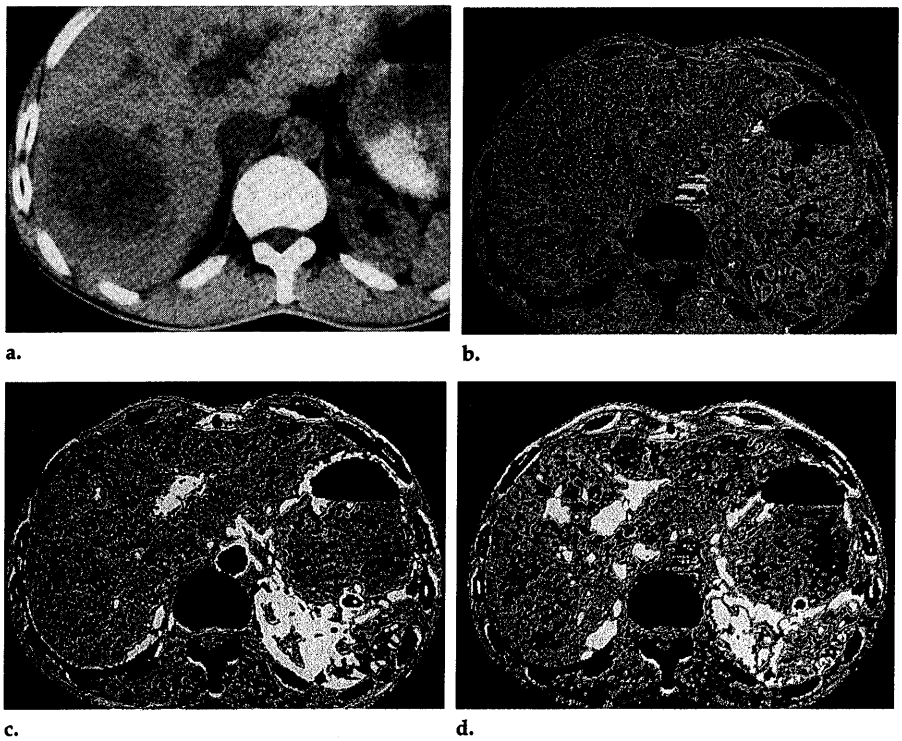

Figure 6. Hepatic metastasis. **(a)** Unenhanced CT scan, **(b)** HPI image, **(c)** arterial perfusion image, and **(d)** portal perfusion image. Note high arterial and low portal perfusion in the metastasis in the right lobe. The remainder of the liver also demonstrates an increased HPI.

and portal veins. Doppler studies primarily provide measurement of blood velocity, and conversion to the more physiologically important volume flow adds substantial inaccuracies.

The CT technique benefits from assessing perfusion at the capillary level, which is more directly related to the metabolic requirements of the tissue than the flow in the supplying vessel. Ultimately, MR imaging techniques may be developed to address these problems.

The main limitation of the CT technique is that only one section level can be readily studied. Thus, although regional variations in the axial plane can be studied, craniocaudal variations may be missed. In addition, the radiation burden of the technique is not inconsiderable; this prevents a greater frequency of data acquisitions (which is technically possible with the Somatom Plus unit). The sequence of data acquisitions used in this study was chosen as a compromise between sample frequency and radiation exposure. After an initial pause to allow passage of contrast material through the heart and lungs, the interval between acquisitions is shorter early in the sequence when changes in enhancement are occurring most rapidly, with greater spacing later when changes occur at a lower rate.

The greatest potential source of error is patient movement during the single-location sequence; this prevented analysis in one patient. Structures with higher or lower attenuation values moving into and out of the section under study between acquisitions alter the recorded attenuation values because of the varying partial-volume effect. The sensation of flushing caused by the injection of the bolus of contrast medium is particularly prone to cause patient movement. This can be minimized by using low-osmolarity agents and carefully instructing the patient and, in practice, rarely degrades the functional images to any extent.

When generating TDCs from very small regions or individual pixels, photon noise becomes an important consideration. Random variations in photon numbers and detector response cause variability in measured attenuation values and, hence, errors in the calculated perfusion values. Use of a soft-tissue reconstruction algorithm (low noise) and compression of the data into a 256 × 256 matrix reduce this effect while maintaining good spatial resolution. We have evaluated this effect by performing dynamic CT in a water phantom. The error in the perfusion measurements depends on the value of perfusion itself; the error is greater with low perfusion. With the Somatom Plus unit, the error resulting from photon noise for an individual pixel (256 × 256) with a typical perfusion value of 0.32 mL/min/mL is ±0.06 mL/min/mL. For perfusion values from a larger ROI (eg, 50 or more pixels as

used in the ROI analysis described earlier), photon noise will be negligible and measurements will be much more precise. Therefore, for quantification of abnormalities detected on functional images, ROI analysis should be performed by using the functional image to guide the creation of the ROI.

Inaccuracies in the timing of peak splenic enhancement could cause errors in the differentiation of the arterial and portal phases; this was a problem for early radionuclide studies with nonextracted tracers (5). However, unlike the radionuclide techniques that integrate the slope over several seconds, the CT method requires the *maximum* slope to be measured. The maximum slope occurs some seconds before (mean, 9.1 seconds) and after (mean, 6.2 seconds) peak splenic enhancement (Fig 1, Table 1); thus, errors in timing of the peak must be large before they affect the measurements. In practice, this does not seem to occur.

We did not use a mechanical pump injector to administer contrast medium. A narrow bolus is important but can be achieved by hand injection, which typically enables 50 mL to be injected within 7–10 seconds. A more rapid injection may not result in a narrower bolus because of bolus spreading in the lungs (25). The bolus shape will also be altered by the speed of injection and the cardiac output and central blood volume of the patient and, thus, a constant bolus cannot be guaranteed with pump injection. A wider bolus with a lower aortic peak will produce a lower rate of enhancement in the tissues; thus, the effects of variations in bolus shape are self-cancelling.

Contrast media are known to be vasodilatory, an effect that relates to their osmolarity. This could increase the perfusion within any organs being studied. However, the effect is unlikely to be substantial within the first pass of the contrast medium, and the use of low-osmolarity agents further reduces any likelihood of such an effect.

There are many potential clinical uses of CT perfusion measurements in the liver. The likely cause of the hemodynamic changes in any given patient will depend in part on the clinical context. Diffuse liver disease, such as cirrhosis, could be detected from perfusion changes, even when the liver appears morphologically normal. In patients with known diffuse liver disease, the quantification allows assessment of severity and comparison of measurements before and after intervention. In patients undergoing CT to exclude hepatic metastases, increased arterial perfusion in a morphologically normal liver would suggest micrometastases that would otherwise go undetected, although liver biopsy might be required for confirmation. Vascular problems after liver transplantation are not uncommon, and the severity of portal or arterial stenosis can be assessed at the capillary level and, unlike with Doppler US, regional variations in hemodynamics are readily evaluated. The quantification of arterial and portal perfusion enables the effects of drugs to be measured, such as drugs aimed at treatment of cirrhosis by modifying blood flow. The ability to create functional maps of perfusion parameters also enables evaluation of focal lesions, such as liver tumors. The study and possible modification of tumor perfusion is of increasing importance to oncologists, as altering the perfusion may "sensitize" metastases to radiation therapy or chemotherapeutic drugs.

CT perfusion imaging of the liver provides quantifiable functional images of several perfusion parameters with a spatial resolution not yet achieved with other imaging techniques.

APPENDIX

The method for deriving tissue perfusion is based on the determination of blood flow as a proportion of cardiac output using radiolabeled microspheres. A time-activity curve over an organ after a bolus injection of microspheres into the left ventricle will rise and reach a maximum height H (in counts per second). The equation for determining blood flow as a proportion of cardiac output is as follows:

$$\frac{OBF}{CO} = \frac{H \times a}{\text{dose injected,}} \qquad \text{(A1)}$$

where OBF is the organ blood flow and CO the cardiac output. (The dose injected will be measured in megabecquerels; a is a correction factor relating centimeters per second to megabecquerels as determined by detector efficiency and photon attenuation.)

The shape of the integrated arterial time-activity curve, corrected for recirculation with a gamma function fit, is the same as that obtained from the organ using microspheres but reaching the plateau at a value A (in counts) and with a maximal slope $g_{arterial}$ (in counts per second). A is also the area under the arterial curve before integration; $g_{arterial}$ is its maximum height. The integrated arterial curve and the organ curve will be related as follows:

$$\frac{g_{organ}}{g_{arterial}} = \frac{H}{A}, \qquad \text{(A2)}$$

where g_{organ} is the maximal slope of the organ time-activity curve (in centimeters per second per second). However, a tracer that is not completely extracted by the organ on its first pass, such as Tc-99m diethylenetriaminepentaacetic acid, will produce a time-activity curve that will not reach this plateau value; however, its maximal slope g_{organ} will be the same as that obtained with microspheres. Thus, if we use Equation (A2) to substitute for H in Equation (A1),

$$\frac{OBF}{CO} = \frac{A}{\text{dose injected}} \times \frac{g_{organ}}{g_{arterial}} \times a. \qquad \text{(A3)}$$

Intravascular contrast media have pharmacokinetic properties that are very similar to those of diethylenetriaminepentaacetic acid and, thus, this method of analysis can be applied to dynamic CT by determining the temporal changes in contrast medium concentration within the aorta and tissue to be studied from their respective TDCs. The correction factor a is not required with CT, as A is measured in Hounsfield units multiplied by minutes and the dose injected can be expressed in Hounsfield units multiplied by milliliters. (An iodine concentration of 1 mg/mL is equivalent to 25 HU; thus, 1 mg of iodine is equivalent to 25 HU · mL.) Because concentration (ie, the amount of iodine per milliliter of tissue) is measured instead of total organ iodine, it is blood flow per milliliter of tissue, or perfusion, that is determined. Thus, for CT:

$$\frac{OBF \text{ per milliliter of tissue}}{CO} = \frac{A}{\text{dose}} \times \frac{g_{organ}}{g_{arterial}} \qquad \text{(A4)}$$

Furthermore, because the cardiac output can be determined with dynamic CT from the injected dose of iodine and the area under the arterial TDC after correction for recirculation A by dividing the dose injected by the area under the arterial TDC, the tissue perfusion is thus calculated as $g_{organ}/g_{arterial}$. g_{organ} is derived from the maximum gradient of tissue TDC and $g_{arterial}$ is given by the peak height of the arterial TDC (before integration and after subtraction of the attenuation value obtained before administration of contrast material). ■

References

1. Peters AM, Gunasekera RD, Henderson BL, et al. Non-invasive measurements of blood flow and extraction fraction. Nucl Med Commun 1987; 8:823–837.
2. Peters AM, Brown J, Hartnell GG, Myers MJ, Haskell C, Lavender JP. Non-invasive measurement of renal blood flow with ^{99m}Tc DTPA: a comparison with radiolabelled microspheres. Cardiovasc Res 1987; 21:830–834.

3. Miles KA. Measurement of tissue perfusion by dynamic computed tomography. Br J Radiol 1991; 64:409–412.
4. Miles KA, Hayball M, Dixon AK. Colour perfusion imaging: a new application of computed tomography. Lancet 1991; 337: 643–645.
5. Sarper R, Fajman WA, Rypins EB, et al. A noninvasive method for measuring portal venous/total hepatic blood flow by hepatosplenic radionuclide angiography. Radiology 1981; 141:179–184.
6. Fleming JS, Ackery DM, Walmsley BH, Karran SJ. Scintigraphic estimate of arterial and portal blood supply to the liver. J Nucl Med 1983; 24:1108–1113.
7. Parkin A, Robinson PJ, Baxter P, Leveson SH, Wiggins PA, Giles GR. Liver perfusion scintigraphy: method, normal range and laparotomy correlation in 100 patients. Nucl Med Commun 1983; 4:395–402.
8. Britten AJ, Fleming JS, Flowerdew ADS, Taylor I, Karran SJ, Ackery DM. Regional indices of relative hepatic arterial perfusion from dynamic liver scintigraphy: the variability of indices and the use of parametric imaging. Nucl Med Commun 1990; 11:29–36.
9. Wraight EP, Barber RW, Ritson A. Relative hepatic arterial and portal flow in liver scintigraphy. Nucl Med Commun 1982; 3:273–279.
10. Axel L. Cerebral blood flow determination by rapid-sequence computed tomography. Radiology 1980; 137:679–686.
11. Shih TTF, Huang KM. Acute stroke: detection of changes in cerebral perfusion with dynamic CT scanning. Radiology 1988; 169:469–474.
12. Jaschke W, Sievers RS, Lipton MJ, Cogan MG. Cine-computed tomographic assessment of regional renal blood flow. Acta Radiol 1989; 31:77–81.
13. Wolfkiel CJ, Ferguson JL, Chomka EV, et al. Measurement of myocardial blood flow by ultrafast computed tomography. Circulation 1987; 76:1262–1273.
14. Gould RG, Lipton MJ, McNamara MT, Sievers RE, Koshold S, Higgins CB. Measurement of regional myocardial blood flow in dogs by ultrafast CT. Invest Radiol 1988; 23:348–353.
15. Berninger WH, Axel L, Norman D, Napel S, Redington RW. Functional imaging of the brain using computed tomography. Radiology 1981; 138:711–716.
16. Nagata K, Asano T. Functional image of dynamic computed tomography for the evaluation of cerebral haemodynamics. Stroke 1990; 21:882–889.
17. Partanen KPL. Dynamic CT of liver cirrhosis. Invest Radiol 1984; 19:303–308.
18. Ternberg JL, Butcher HR Jr. Blood-flow relation between hepatic artery and portal vein. Science 1965; 150:1030–1031.
19. Ferguson DJ. Haemodynamics in surgery for portal hypertension. Ann Surg 1963; 158:383–386.
20. Itai Y, Moss AA, Goldberg HI. Transient hepatic attenuation difference of lobar or segmental distribution detected by dynamic computed tomography. Radiology 1982; 144:835–839.
21. Chan SCH, Chan F-L, Chau EMT, Mok FPT. Portal thrombosis complicating appendicitis: ultrasound detection and hepatic computed tomography lobar attenuation alteration. J Comput Tomogr 1988; 12: 208–210.
22. Mathieu D, Vasile N, Dibie C, Grenier P. Portal cavernoma: dynamic CT features and transient differences in hepatic attenuation. Radiology 1985; 154:743–748.
23. Mathieu D, Vasile N, Fagniez P-L, Segui S, Grably D, Larde D. Dynamic CT features of hepatic abscesses. Radiology 1985; 154: 749–752.
24. Leveson SH, Wiggins PA, Giles GR, Parkin A, Robinson PJ. Deranged liver blood flow patterns in the detection of liver metastases. Br J Surg 1985; 72:128–130.
25. Claussen C, Lochner B. Bolus geometry and dynamics: contrast studies with intravenous contrast media. In: Dynamic computed tomography: basic principles and clinical applications. Berlin, Germany: Springer-Verlag, 1985; 33–37.